

# Single-Nitrogen-vacancy-center quantum memory for a superconducting flux qubit mediated by a ferromagnet

Yen-Yu Lai,<sup>1,2</sup> Guin-Dar Lin,<sup>1,2</sup> Jason Twamley,<sup>3</sup> and Hsi-Sheng Goan<sup>1,2,\*</sup>

<sup>1</sup>*Department of Physics and Center for Theoretical Physics,  
National Taiwan University, Taipei 10617, Taiwan*

<sup>2</sup>*Center for Quantum Science and Engineering, National Taiwan University, Taipei 10617, Taiwan*

<sup>3</sup>*Centre for Engineered Quantum Systems, Department of Physics and Astronomy, Macquarie University, NSW 2109, Australia*

(Dated: May 1, 2018)

We propose a quantum memory scheme to transfer and store the quantum state of a superconducting flux qubit (FQ) into the electron spin of a single nitrogen-vacancy (NV) center in diamond via yttrium iron garnet (YIG), a ferromagnet. Unlike an ensemble of NV centers, the YIG moderator can enhance the effective FQ-NV-center coupling strength without introducing additional appreciable decoherence. We derive the effective interaction between the FQ and the NV center by tracing out the degrees of freedom of the collective mode of the YIG spins. We demonstrate the transfer, storage, and retrieval procedures, taking into account the effects of spontaneous decay and pure dephasing. Using realistic experimental parameters for the FQ, NV center and YIG, we find that a combined transfer, storage, and retrieval fidelity higher than 0.9, with a long storage time of 10 ms, can be achieved. This hybrid system not only acts as a promising quantum memory, but also provides an example of enhanced coupling between various systems through collective degrees of freedom.

PACS numbers: 03.65.Yz, 42.50.Dv, 03.67.-a, 03.65.Ta

## I. INTRODUCTION

Superconducting qubits and related circuit-QED devices [1, 2] with excellent scalability, parametric tunability, and strong coupling with external fields are proving to be a powerful platform for quantum information processing. However, they suffer from decoherence due to inevitable interactions with their surrounding environments. In a complex quantum protocol, superconducting qubits may experience frequent idles times when they are not involved in active quantum gates. During this idle time, to prevent the decoherence of their quantum information, one can transfer their quantum state to an adjacent quantum memory for better protection.

A hybrid system that takes advantage of the fast operation of superconducting qubits and long coherence times of a suitable quantum memory may yield good coherence preservation if the state transfer between them is quick enough, i.e., faster than the decoherence time of either system. The spin of a nitrogen-vacancy (NV) center in diamond, which has a relatively long coherence time even at room temperature [3], can be a candidate for such a quantum memory. This low decoherence rate also means that the NV center normally only couples weakly to a superconducting qubit. Such a weak coupling leads to a slow state transfer and coherence loss can be significant. Ensembles of NV centers [4–8] may make the coupling stronger, but at the added cost of increased decoherence caused by internal spin-spin interactions, degrading the fidelity of the quantum memory.

In this paper, we propose a scheme to transfer quantum states faithfully between a superconducting flux qubit and a single-NV-center spin via the ferromagnetic material yttrium iron garnet (YIG) [9, 10]. YIG has been proposed as a mediator for classical magnetic fields to enhance the sensitivity of a NV magnetometer to achieve single nuclear spin detection [11]. In addition, the large number of spins in YIG with strong exchange interaction leads to collective-excitation modes with narrow linewidths at low temperature [12, 13]. These collective modes are known as quasiparticles or magnons [14], and have been shown to be capable of coupling to different kinds of quantum systems, such as superconducting microwave cavity modes [13, 15, 16]. Magnons in YIG have also been proposed as a mediator of coherent coupling between two distant spins (e.g., two spatially distant NV-center spins) [17]. A CNOT gate between two single-NV-center spins separated by a distance of about  $1 \mu\text{m}$  with operation times of the order of a few tens of nanoseconds has been demonstrated [17]. This shows that a relatively strong coherent coupling between a single-NV-center spin and YIG magnons is feasible. On the other hand, a flux qubit (FQ) can display strong coherent coupling to an ensemble of NV centers exhibiting a collective coupling of  $\sim 70 \text{ MHz}$  [8]. However the spin density of YIG ( $\rho \sim 4.2 \times 10^{21} \text{ cm}^{-3}$ ) [13] is almost three orders of magnitude larger than typical NV ensembles ( $\rho \sim 5 \times 10^{18} \text{ cm}^{-3}$ ) [8]. This suggests that the coupling between a flux qubit and a small YIG sample may be similar or even stronger than between a flux qubit and a NV ensemble. In this paper, we show that we can achieve a substantially large effective coupling between a single-NV-center spin and a FQ by using the magnons in a small nearby YIG sample as a mediator without appreciably sacrificing the transfer

\* goan@phys.ntu.edu.tw

and storage fidelity of the quantum state.

When the size of the YIG is small enough, the Kittel mode (KM) of the YIG sample [13, 15] is gapped from the higher-energy modes and thus plays an important role in a low-temperature and low-excitation regime. In our scheme, we find that the effective coupling and the spatial separation between the FQ and NV required to attain these coupling strengths via the YIG can be significantly enhanced. The coupling attained using our proposal is of the order of several tenths of MHz, while the spatial separation can be increased to a few tenths of  $\mu\text{m}$ . This represents an enhancement in the coupling strength of 3–7 times over the direct FQ-NV coupling. More interestingly, it also represents a substantial enhancement in spatial separation required between the FQ and NV. For comparison, a direct coupling scheme [18] finds a coupling strength of  $\sim 100$  kHz, but requires a minuscule spatial separation of 20 nm. To achieve larger direct coupling strength, strengths comparable to those found using our scheme would require even tinier spatial separations, which may be physically unrealistic. In contrast, in our proposal we are able to expand the spatial separation to a few tenths of a  $\mu\text{m}$  scale, which is 10–20 times larger than the separation required to attain similar coupling strengths via direct FQ-NV coupling. Thus our scheme can provide significant couplings over a separation, which is technically far easier to engineer. The quantum state transfer time with the coupling strength found in our scheme is considerably smaller than the decoherence time of the FQ so that fast and faithful transfer can be realized without suffering significant decoherence.

The paper is arranged as follows. In Sec. II, we derive the effective Hamiltonian and coupling strength between a FQ and a NV-center spin from a FQ-YIG-NV-center hybrid system. In Sec. III, we introduce a protocol for the transfer and storage of the quantum state. After that, simulations of the protocol are presented and discussed in Sec. IV, taking major decoherence effects into consideration. Finally, a short conclusion is given in Sec. V. All the details of derivations of equations and calculations are presented in Appendices A and B.

## II. MODEL

The hybrid system in our proposal is schematically illustrated in Fig. 1 and contains three parts: the FQ, YIG, and a single-NV center. The noninteracting Hamiltonian describing the individual systems [with  $(\hbar = 1)$ ] can be written as

$$H_s = H_F + H_Y + H_N, \quad (1)$$

where

$$H_F = \frac{1}{2}\omega_F\sigma_F^{(z)}, \quad (2)$$

$$H_Y = -J \sum_{\langle r, r' \rangle} S_r \cdot S_{r'} + \gamma_e B \sum_r S_r^{(z)}, \quad (3)$$

$$H_N = \Delta_{\text{ZS}} \left( S_N^{(z)} \right)^2 - \gamma_e B S_N^{(z)}. \quad (4)$$

Here, the FQ is regarded as a typical two-level system described by the Hamiltonian  $H_F$  in Eq. (2), with  $\omega_F$  the transition frequency of the FQ and  $\sigma^{(z)}$  the Pauli matrix (for details, see Appendix A). The Hamiltonian of the YIG in an external field along the  $z$  axis is given by  $H_Y$  in Eq. (3), where  $S_r$  are the operators of the spin located at position  $r$  in the YIG. The parameter  $J$  is the exchange coupling between the spins inside the YIG. We consider the application of  $B = B_L + \delta B$ , an external magnetic field along the  $z$  axis and which is felt by the YIG and the NV center (see Fig. 1 and 2). Here,  $B_L$  is a local magnetic field generated by a micromagnet [19] without disturbing the FQ (for details, see Sec. IV), and  $\delta B$  is the tuneable magnetic field whose value is set below the critical field of the FQ. The tuneable dc magnetic field could be generated by a coil. The ground triplet states of the NV center is described by the Hamiltonian  $H_N$  in Eq. (4), where  $S_N^{(z)}$  is the  $z$  component of the spin-1 operators of the single-NV center,  $\Delta_{\text{ZS}} = 2.87$  GHz is the zero-field splitting of the ground triplets, and  $\gamma_e = -1.76 \times 10^{11}$  rad s $^{-1}$  T $^{-1}$  is the gyromagnetic ratio of electron spin. To proceed further, let us simplify the Hamiltonians a little bit. There are two single-photon transitions between  $|0_N\rangle$  and  $|\pm 1_N\rangle$  in the ground triplet states of the NV-center spin, and their energy gaps are  $\omega_{(\pm 1)} = \Delta_{\text{ZS}} \mp \gamma_e B$ . We use, for instance, the NV-center spin states  $|0_N\rangle$  and  $|-1_N\rangle$  as our storage qubit basis state. In the state transfer stage, this transition frequency is tuned to be resonant with the FQ transition frequency, while the  $|0_N\rangle$  to  $|1_N\rangle$  transition is largely detuned (see Fig. 2). Further, as shown later, the effective coupling between the FQ and the NV-center storage qubit can be switched on and off (or very small) by varying the external  $B$  field. Here, for the sake of deriving the effective Hamiltonian, we first treat the NV-center spin as a two-level storage qubit by ignoring the far-detuned transition. We will take into account the effect of the existence of the far-detuned NV  $|1_N\rangle$  state when we run numerical simulations for the dynamics of quantum state transfer and storage processes. We then transform the YIG Hamiltonian from a Heisenberg model to a magnon form with the Holstein-Primakoff transformation [17, 20, 21] and harmonic approximation. As a result, the NV and YIG Hamiltonians can be rewritten as [17, 21]

$$H_N \simeq \frac{1}{2}\omega_N\sigma_N^{(z)}, \quad (5)$$

$$H_Y \simeq \sum_k \omega_k a_k^\dagger a_k, \quad (6)$$

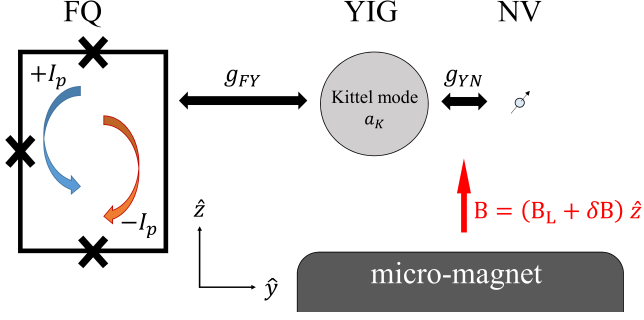


Figure 1. Schematic illustration of the proposed quantum memory. The FQ is regarded as a two-level system depending on the sign (direction) of its persistent current  $I_p$ , and the KM in YIG couples to both FQ and the single-NV-center spin with strengths  $g_{FY}$  and  $g_{YN}$ , respectively. The external magnetic field felt by the YIG and the NV center is  $B = B_L + \delta B$  (see Fig. 2), where  $B_L$  is a local magnetic field generated by a micromagnet without disturbing the FQ, and  $\delta B$  is a tuneable magnetic field, generated by, e.g., a coil.

where  $\omega_N = \omega_{(-)}$ , and  $\omega_k = sJa^2k^2 + \gamma_e B$  are the frequencies of the NV storage qubit and magnon mode  $k$ , respectively,  $a_k^\dagger$  ( $a_k$ ) is the creation (annihilation) operator of magnon mode  $k$ ,  $s$  is the maximum eigenvalue of the spin operator  $S_r^{(z)}$ , and  $a$  is the lattice constant of the YIG. For a small-sized YIG sample, the boundary conditions at the surface are of great importance and the magnon modes become gapped.

The FQ and NV interact indirectly via YIG. The coupling Hamiltonian thus has two parts: the FQ-YIG coupling and the YIG-NV coupling. The current in the loop of the FQ generates a magnetic field which interacts with the spins in the YIG. The NV electron spin also couples to these spins by dipole-dipole interaction. Under the rotating-wave approximation (RWA), the coupling Hamiltonian in terms of the YIG collective-excitation modes (derived in detail in Appendix A) reads

$$H_c = H_{FY} + H_{YN}, \quad (7)$$

$$H_{FY} \simeq - \sum_k \left( g_{FY}(k) \sigma_F^{(+)} a_k + H.C. \right), \quad (8)$$

$$H_{YN} \simeq - \sum_k \left( g_{YN}(k) a_k^\dagger \sigma_N^{(-)} + H.C. \right), \quad (9)$$

where

$$g_{FY}(k) = \frac{\mu_0}{2\pi} \gamma_e I_p \sqrt{\frac{2s}{N}} \sum_{r_F}^N \frac{e^{-ik \cdot a}}{r_F}, \quad (10)$$

$$g_{YN}(k) = - \frac{\mu_0}{4\pi} \gamma_e^2 \hbar \sqrt{\frac{2s}{N}} \sum_{r_N}^N \left( \frac{3\cos^2\theta_{r_N} - 1}{r_N^3} \right) e^{ik \cdot a}, \quad (11)$$

are the coupling strength of the FQ and NV with magnon mode  $k$  in the YIG, respectively. Here,  $\mu_0$  is the vacuum permeability,  $I_p$  is the persistent current of the FQ,  $r_F$

( $r_N$ ) is the distance between a spin in the YIG and the FQ (the NV spin),  $N$  is the number of the spins in the YIG, and  $\theta_{r_N}$  is the angle between the vector connecting the NV and the spin in YIG, and the direction of the external magnetic field. Under the condition that the Heisenberg interaction inside the YIG is much greater than the coupling between a qubit and any single spin in the YIG, the qubit then effectively interacts with the collective mode of all the spins in the YIG. The more spins in the YIG following this condition, the stronger the coupling.

If one chooses a YIG sphere with a submicrometer diameter, then the energy levels of the YIG magnon modes are gapped, largely due to its small size. We consider only the simplest mode of the YIG, i.e., the KM [13, 15], with frequency  $\omega_K$  which is far from both the frequencies of the FQ and NV-center storage qubit. Thus the KM is in a virtual coupling regime with the FQ and NV-center storage qubit. To account for the overall effect, we use the Schrieffer-Wolff transformation (SWT) to derive the effective Hamiltonian up to the second order in the coupling strengths with the YIG by averaging out the far-off-resonance degrees of freedoms of the YIG. We then obtain (with detailed derivation shown in Appendix B) an effective Hamiltonian between the FQ and the NV-center qubit as

$$H_{\text{eff}} \simeq \frac{1}{2} \omega_{F,\text{eff}} \sigma_F^{(z)} + \frac{1}{2} \omega_{N,\text{eff}} \sigma_N^{(z)} + g_{FN,\text{eff}} \left( \sigma_F^{(+)} \sigma_N^{(-)} + H.C. \right), \quad (12)$$

where

$$\omega_{F,\text{eff}} = \omega_F + \delta_F, \quad (13)$$

$$\omega_{N,\text{eff}} = \omega_N + \delta_N, \quad (14)$$

are the effective frequencies of the FQ and the NV-center storage qubit with frequency shifts  $\delta_F = \frac{g_{FY}^2(\omega_K)}{\omega_F - \omega_K}$  and  $\delta_N = \frac{g_{YN}^2(\omega_K)}{(\omega_N + \delta_{YN}) - \omega_K}$  induced by the KM of the YIG, respectively, and

$$g_{FN,\text{eff}}(\omega_K) = \frac{1}{2} g_{FY}(\omega_K) g_{YN}(\omega_K) \times \left[ \frac{1}{\omega_F - \omega_K} + \frac{1}{(\omega_N + \delta_{YN}) - \omega_K} \right] \quad (15)$$

is the effective coupling strength between the FQ and the NV-center qubit. Here,  $\omega_K$  denotes the frequency of the KM. Note that to have a substantially large effective coupling, the detuning  $(\omega_F - \omega_K)$  and detuning  $(\omega_N + \delta_{YN} - \omega_K)$  appearing in the denominator of Eq. (15) should not be too large. On the other hand, to keep the KM in a regime of virtual coupling with the FQ and NV-center storage qubit, they should not be too small. By varying the external magnetic field, we can control the values of  $(\omega_F - \omega_K)$  and  $(\omega_N - \omega_K)$ . In particular, the change in  $\omega_K$ , due to the variation of the magnetic

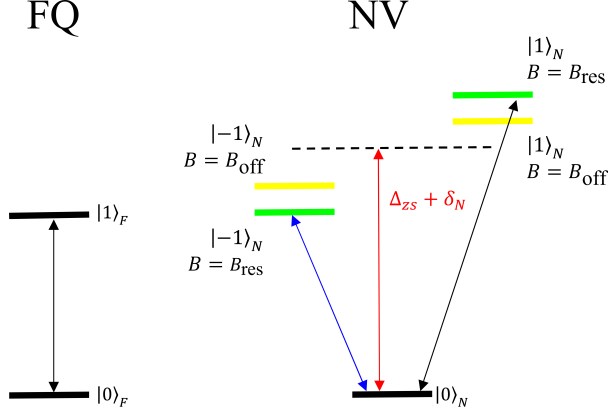


Figure 2. Energy-level diagram of the FQ (left) and the ground triplet states of the NV-center spin (right). The NV-center spin states  $|\pm 1_N\rangle$  are degenerate (dashed line) and have a zero-field splitting  $\Delta_{ZS}$  and an energy shift  $\delta_N$  induced by the indirect coupling scheme via YIG relative to state  $|0_N\rangle$  (see red arrow). By tuning the magnetic field on the NV-center spin to the value of  $B = B_{\text{res}}$ , one can control the transition between  $|0_N\rangle$  and  $|-1_N\rangle$  to be resonant with the FQ (see blue arrow) or to be off-resonant at  $B = B_{\text{off}}$ . The transition between  $|0_N\rangle$  and  $|1_N\rangle$  is always set to be off-resonant with the FQ, i.e., is set to be a disconnected channel.

field, is opposite to the change of the energy difference between  $|0_N\rangle$  and  $|-1_N\rangle$  [in contrast to the same energy change between  $|0_N\rangle$  and  $|1_N\rangle$  resulting in no change in  $(\omega_{(+1)} - \omega_K)$ ]. This makes  $|0_N\rangle$  and  $|-1_N\rangle$  a better choice of storage qubit basis states.

### III. QUANTUM MEMORY

Next we will use the derived effective Hamiltonian to investigate the dynamics and the fidelity of the proposed quantum memory scheme. There are two stages that we need to consider: state transfer stage and state storage stage.

To better assess and calculate the fidelity of our scheme, we take all the lowest triplet states of the NV spin into account. In this case, the FQ couples to two transitions in these triplets separately and the effective Hamiltonian, given by Eq. (12), becomes

$$\begin{aligned}
 H_{\text{eff}} = & \frac{1}{2} \omega_{F,\text{eff}} \sigma_F^{(z)} + \sum_{j=\pm 1} \omega_{N,(j),\text{eff}}(B) |j_N\rangle \langle j_N| \\
 & + g_{(+1)} \left[ \sigma_F^{(+)} S_{N,(+1)}^{(-)} + H.C. \right] \\
 & + g_{(-1)} \left[ \sigma_F^{(+)} S_{N,(-1)}^{(-)} + H.C. \right], \quad (16)
 \end{aligned}$$

Here in the spin-1 Hilbert space of the NV center, the effective NV spin frequencies are  $\omega_{N,(\pm 1),\text{eff}}(B) = \Delta_{ZS} \mp \gamma_e B + \delta_{N,(\pm 1)}$ , where  $\Delta_{ZS}$  is the zero-field splitting and  $\delta_{N,(\pm 1)}$  is the frequency shift. The effective coupling

strengths between the FQ and the NV spin transitions are denoted as  $g_{(\pm 1)}$ , corresponding to Eq. (15) with  $\omega_N \rightarrow \omega_{N,(\pm 1),\text{eff}}(B)$ . The subscripts  $(\pm 1)$  in the expression (and in the following), stand for the transitions between  $|0_N\rangle$  and  $|\pm 1_N\rangle$ , respectively. The operators  $S_{N,(\pm 1)}^{(\pm)}$  with superscript  $\pm$  denote the raising and lowering operators, respectively.

Now we move to the interaction picture through the unitary transformation  $U = \exp(-itH_{0,\text{eff}})$ , where  $H_{0,\text{eff}} = \frac{1}{2} \omega_{F,\text{eff}} \sigma_F^{(z)} + \sum_{j=\pm 1} \omega_{N,(j),\text{eff}}(B_{\text{res}}) |j_N\rangle \langle j_N|$  is the first two terms of the effective Hamiltonian given by Eq. (16) with magnetic field  $B = B_{\text{res}}$ , where  $B_{\text{res}}$  is the magnetic field strength applied to the NV-center spin when the transition between  $|0_N\rangle$  and  $|-1_N\rangle$  matches the energy gap of the FQ (see Fig. 2). Then the effective interaction Hamiltonian  $H_{\text{int}}$  becomes

$$H_{\text{int}} = H_{N,\text{int}} + H_{FN,\text{int}}, \quad (17)$$

$$H_{N,\text{int}} = \sum_{j=\pm 1} \delta_{B,(j)} |j_N\rangle \langle j_N|, \quad (18)$$

$$\begin{aligned}
 H_{FN,\text{int}} = & g_{(-1)} \left[ \sigma_F^{(+)} S_{N,(-1)}^{(-)} + H.C. \right], \\
 & + g_{(+1)} \left[ \sigma_F^{(+)} S_{N,(+1)}^{(-)} e^{2it\gamma_e B_{\text{res}}} + H.C. \right], \quad (19)
 \end{aligned}$$

and

$$\delta_{B,(\pm 1)} = \mp \gamma_e (B - B_{\text{res}}). \quad (20)$$

When  $\delta_{B,-1}$  is tuned to zero, i.e.,  $B = B_{\text{res}}$ , the  $g_{(-1)}$  coupling terms start to transfer the quantum state from the FQ to the NV-center spin and the fast oscillating components in the  $g_{(+1)}$  terms can be effectively neglected.

We initially prepare the NV in the ground state,  $|\psi_N(0)\rangle = |0_N\rangle$ . Suppose that the FQ is in a general state characterized by angles  $\theta$  and  $\phi$ . Then the joint state is

$$\begin{aligned}
 |\psi(0)\rangle = & (\cos \theta |1_F\rangle + e^{i\phi} \sin \theta |0_F\rangle) \otimes |0_N\rangle \\
 = & \cos \theta |1_F, 0_N\rangle + e^{i\phi} \sin \theta |0_F, 0_N\rangle. \quad (21)
 \end{aligned}$$

After a transfer time  $t = \pi/(2g_{(-1)})$ , the target state in the interaction picture becomes

$$\begin{aligned}
 |\psi(t)\rangle = & -i \cos \theta |0_F, -1_N\rangle + e^{i\phi} \sin \theta |0_F, 0_N\rangle \\
 = & |0_F\rangle \otimes (-i \cos \theta |-1_N\rangle + e^{i\phi} \sin \theta |0_N\rangle). \quad (22)
 \end{aligned}$$

Once the state has been transferred to the NV-center spin, we turn off the coupling effectively by enlarging the mismatch of the frequencies between the FQ and the NV-center storage qubit. The quantum state can thus be stored for better coherence with dephasing time characterized by the NV-center spin's  $T_2$  time. To retrieve the state from the NV-center storage qubit to the FQ, we tune to the NV-FQ resonance again. After a time  $t_1 = \pi/(2g_{(-1)})$ , the original state is restored in the FQ degrees of freedom

$$|\psi(t_f)\rangle = -e^{-i\phi_s} \cos \theta |1_F, 0_N\rangle + e^{i\phi} \sin \theta |0_F, 0_N\rangle, \quad (23)$$

with an additional phase  $\phi_s$  that comes from the coherent evolution during the storage time  $t_2$  and since this is known it can be corrected.

#### IV. RESULTS AND DISCUSSION

We present the numerical results together with discussions to verify our scheme here. Before proceeding with our numerical calculations for the fidelity performance, we first describe the system parameters used. It is assumed that the YIG is a sphere of radius about 45 nm and contains about  $10^6$  spins. A local magnetic field  $B_L$  is generated by placing a micromagnet [19] of size  $0.2 \times 0.2 \times 0.2 \mu\text{m}^3$  with a uniform perpendicular magnetization of about a hundred Gauss at a vertical distance  $\sim 25\text{--}50$  nm from the YIG. With this local magnetic field, the frequency of the KM can reach GHz levels; furthermore, by varying an external magnetic field the frequency difference ( $\omega_F - \omega_K$ ) can achieve a typical value of about 170 MHz. Since the direction of  $B_L$  is parallel to the plane of the FQ, the FQ is insensitive to  $B_L$ . Furthermore, because the transverse distance from the micromagnet boundary at which  $B_L$  drops to 0, is smaller than  $0.1 \mu\text{m}$  [19], if  $r_F$  is considerably larger than the sum of this transverse distance and the distance from the YIG to the left boundary of the micromagnet (see Fig. 1), we can realize local magnetic field control for the YIG without disturbing the FQ. Therefore, by choosing a relatively large value of  $r_F \sim 0.25 \mu\text{m}$  and using a FQ with  $I_p = 500$  nA and a diamond with a single NV spin at a distance  $r_N \sim 60$  nm from the YIG, we can estimate the effective coupling strength  $g_{FN,\text{eff}}$  to be about 350–700 kHz according to Eqs. (A12), (A14), and (B14). The frequency shifts of both the FQ and NV-center spin due to the YIG coupling [see Eqs. (B8) and (B9)] are at about hundreds kHz, and are thus rather small and negligible in comparison with their own frequencies in the GHz range.

Following the exposition of the system parameters, we now continue to show the numerical results and we plot the dynamics of the transfer process in Fig. 3. We choose the case where the effective coupling strength is 700 kHz and where the initial state is  $|\Phi_{1/2}\rangle = \sqrt{1/2}|1_F, 0_N\rangle + \sqrt{1/2}|0_F, 0_N\rangle$  since this state is, in a more realistic situation considered later, influenced the most by the dephasing effect. During the transfer process (whose duration is  $0.36 \mu\text{s}$ ),  $|1_F, 0_N\rangle$  is transferred to  $|0_F, -1_N\rangle$ , while  $|0_F, 0_N\rangle$  is left unchanged. The population of the other states remains zero, except that the  $|0_F, 1_N\rangle$  state has a small probability ( $\sim 10^{-7}$ ) as shown in Fig. 3(b). This small probability is due to the detuning between the transition frequency from  $|0_N\rangle$  to  $|1_N\rangle$  and the frequency of the FQ, and one can reduce this probability further by making the detuning larger.

To simulate the state transfer and storage processes in a more realistic setting, we use the master equation [22], which takes into account both spontaneous decay

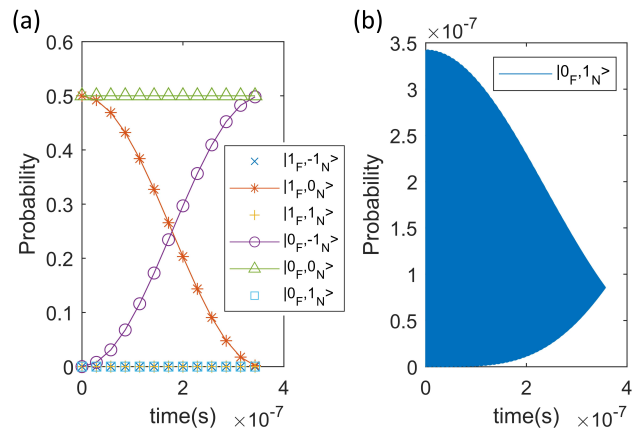


Figure 3. (a) Dynamics of the probabilities of the basis states of the quantum memory during a state transfer process for the initial state  $|\Phi_{1/2}\rangle = \sqrt{1/2}|1_F, 0_N\rangle + \sqrt{1/2}|0_F, 0_N\rangle$ , and coupling strength 700 kHz. During the transfer process,  $|1_F, 0_N\rangle$  is transferred to  $|0_F, -1_N\rangle$ , while  $|0_F, 0_N\rangle$  is unchanged. (b) Due to the detuning between the  $|0_N\rangle$  to  $|1_N\rangle$  transition and the FQ transition frequency, state  $|0_F, 1_N\rangle$  has a negligible probability ( $\sim 10^{-7}$ ) during the process.

and pure dephasing of the FQ and the NV-center spin,

$$\begin{aligned} \frac{d\rho}{dt} = & -i[H_{\text{eff}}, \rho] \\ & + \frac{\gamma_F^{(s)}}{2} \mathcal{L}[\sigma_F^{(-)}] + \frac{\gamma_F^{(p)}}{2} \mathcal{L}[|1_F\rangle\langle 1_F|] \\ & + \sum_{j=\pm 1} \frac{\gamma_{N,(j)}^{(s)}}{2} \mathcal{L}[S_{N,(j)}^{(-)}] + \frac{\gamma_{N,(j)}^{(p)}}{2} \mathcal{L}[|j_N\rangle\langle j_N|], \quad (24) \end{aligned}$$

where  $\mathcal{L}[O] = 2O\rho O^\dagger - \rho O^\dagger O - O^\dagger O\rho$ , is the Lindblad superoperator, and  $\gamma_q^{(s)}$  and  $\gamma_q^{(p)}$  are the spontaneous decay and the dephasing rates, respectively, of the species  $q$ . Note that they are related to the relaxation time  $T_1$  and decoherence time  $T_2$  as  $T_1 = 1/\gamma^{(s)}$  and  $T_2 = 2/(\gamma^{(s)} + 2\gamma^{(p)})$ , respectively [22]. It has been reported recently that both the intrinsic  $T_1^*$  and  $T_2^*$  of FQ's could be about  $10 \mu\text{s}$  at 33 mK [23] and the value of the intrinsic  $T_2^*$  of an NV-center spin could be about  $90 \mu\text{s}$  at room temperature [24]. Furthermore, it has been shown that by applying dynamical decoupling pulse sequences,  $T_1$  of ensembles of NV spins could be more than 10 sec and  $T_2$  could be about 0.6 sec at 77 K [25]. In the simulations, the relevant decoherence times in the state transfer stage are the intrinsic  $T_1^*$  and  $T_2^*$  times of the FQ and the NV-center spin. In the state storage stage, however, the NV-center spin is effectively decoupled from the YIG and FQ due to the large detuning and thus dynamical decoupling pulse sequences can be applied to protect the NV from decoherence to maintain the transferred state. Consequently, we can use the  $T_1$  and  $T_2$  values of the NV-center spin measured using dynamical decoupling [25] to estimate the fidelity in the state storage stage. Furthermore, the decoherence times

of a NV center solely due to a coupling to a ferromagnet YIG have been estimated in Ref. [17], and these times depend sensitively on the ratio of the magnon excitation gap to the YIG temperature. It has been shown that for a magnon gap of  $100 \mu\text{eV}$  and a temperature of  $0.1 \text{ K}$ , these times are typically much larger than the (intrinsic) decoherence times of the NV [17]. In other words, the induced decoherence solely due to coupling to the YIG for temperatures smaller than the magnon excitation gap is nondetrimental [17]. In our scheme, all of the components (the FQ, YIG, and NV) of the qubit and quantum memory are at the same low temperature as that of the FQ. Moreover, because of the small size of the YIG and the applied magnetic field, this ratio of the magnon excitation gap to the temperature in our scheme is even bigger than that used for estimation in Ref. [17]. As a result, the effect of the induced decoherence solely due to coupling to the YIG will be neglected in our simulations.

The effect of the linewidth of the YIG nanosphere can also be neglected. The linewidths of the KM of a single YIG sphere with submillimeter size have been measured to be about  $1\text{--}2 \text{ MHz}$  [12, 13]. Although linewidth measurement on a single YIG nanosphere is, to our knowledge, not available so far, a close case of YIG nanodisks with thickness about  $20 \text{ nm}$  and diameter ranging from  $\sim 300\text{--}700 \text{ nm}$  has been reported in Ref. [26]. There, the linewidth of the uniform mode, i.e., the lowest-energy ferromagnetic resonance mode of a nanodisk, was measured to be about  $7 \text{ MHz}$  for a nanodisk with diameter  $700 \text{ nm}$  at frequency  $8.2 \text{ GHz}$ . However, since this measurement was performed at room temperature and the nanodisks with different diameters are arranged in a row with  $3 \mu\text{m}$  spacing (i.e., not completely a single-disk measurement), one may expect that the linewidth could be narrower if the measurements were performed for a actual single nanodisk at a low temperature of tens of mK and at the frequency down to the value of  $\sim 2 \text{ GHz}$  as in our proposal. Furthermore, the linewidths of the nanodisks do not change much with the diameter [27], at least within the range investigated in Ref. [26]. One may thus expect that the linewidth of a YIG nanosphere without surface defects at low temperature could be similar or at most at a few MHz level, which is still much smaller than the detuning ( $\geq 170 \text{ MHz}$ ) between the YIG nanosphere and other quantum systems in our proposal. Consequently, the effect of the linewidth of the KM of the YIG nanosphere does not appreciably affect the virtual excitation or virtual coupling picture in our proposal and thus is neglected in the subsequent calculations after the degrees of freedoms of the YIG are traced out.

We then take the values of the decoherence and relaxation times at higher temperatures [24, 25] to make a conservative evaluation of the performance of our quantum memory scheme through the fidelity of the state

$$F = \sqrt{\langle \Psi | \rho | \Psi \rangle}, \quad (25)$$

where  $|\Psi\rangle$  is the target state and  $\rho$  is the actual system density matrix. We can transform the Hamiltonian to the

rotating frame to obtain  $H_{\text{int}}$  as in Eqs. (17)–(19). Since during the storage stage the system is tuned to be off-resonant, i.e.,  $\delta_{B,(-1)} \gg g_{(-1)}$ , the total system approximately undergoes free evolution during this stage. The fidelities of the quantum state memory for initial states  $|\Phi_1\rangle$  and  $|\Phi_{1/2}\rangle$  are shown in Table I, in which results that make use of more conservative values for  $T_2^* = 20 \mu\text{s}$  for the NV center are also presented. The initial states  $|\Phi_1\rangle$  and  $|\Phi_{1/2}\rangle$  are chosen because they are influenced the most by the spontaneous decay and dephasing effect, respectively. We have also simulated for different initial states of  $|\Phi_0\rangle = |0_F, 0_N\rangle$ ,  $|\Phi_{1/3}\rangle = \sqrt{2/3}|1_F, 0_N\rangle + \sqrt{1/3}|0_F, 0_N\rangle$ ,  $|\Phi_{1/4}\rangle = \sqrt{3/4}|1_F, 0_N\rangle + \sqrt{1/4}|0_F, 0_N\rangle$ , and  $|\Phi_{1/5}\rangle = \sqrt{4/5}|1_F, 0_N\rangle + \sqrt{1/5}|0_F, 0_N\rangle$ , and the result shows that  $|\Phi_1\rangle$  has the worst fidelity. This is because during the transfer stage, the main factor causing infidelity is the decoherence of the FQ, and  $T_1^*$  and  $T_2^*$  of the FQ is about the same in our case so that the spontaneous decay rate is larger than the dephasing rate. Furthermore, in the transfer stage, switches take place between  $|\Phi_1\rangle = |1_F, 0_N\rangle$  and  $|0_F, -1_N\rangle$ , while the state  $|\Phi_0\rangle = |0_F, 0_N\rangle$  is unchanged. When the portion of  $|\Phi_1\rangle$  in a general initial state decays into  $|0_F, 0_N\rangle$ , the state transfer process of that portion will stop and will cause infidelity. This results in the initial state  $|\Phi_1\rangle$  being the worst possible case for the parameters we used. Nevertheless, if the effective coupling is stronger through the use of a YIG moderator containing more spins or if the FQ possesses a longer coherence time [28], the fidelity can be appreciably enhanced.

In our scheme, the state transfer interaction can be effectively turned on and off depending on whether or not the NV storage qubit is resonant with the FQ. We thus can attempt to consider engineering a near-perfect step function of the external magnetic field  $\delta B$  from  $0 \text{ G}$  (off) to  $80 \text{ G}$  (on). We choose the maximum magnetic field strength such that it is still lower than the critical field of the FQ (the critical field is  $100 \text{ G}$  for FQ made of aluminum; could be higher if made of other superconductor)[29]. However, due to technical limits on the charging and discharging times of circuits, the ramping of the magnetic field cannot be instantaneous and we take this rise time into account. We assume a variation of the magnetic field over  $200 \text{ G}$  in  $10 \text{ ns}$ , similar to what has been reported in experiments [30]. In our simulation,  $\delta B$  is switched from  $0$  to  $80 \text{ G}$  with either a linear or exponential ramping over a duration of  $4$  and  $10 \text{ ns}$  (see Fig. 4). The results shown in Table II indicate that the linear ramping has slightly lower fidelity than the exponential ramping. This is due to the fact that the linear ramping makes the system stay in the near-resonance regime longer and thus subject to FQ decoherence longer. Shorter rise times of the magnetic field can also improve the fidelity or, alternatively, one can fine tune the transfer time to correct the rise-time and fall-time effects.

Table I. Fidelity at different steps for the initial states of  $|\Phi_1\rangle = |1_F, 0_N\rangle$  and  $|\Phi_{1/2}\rangle = \sqrt{1/2}|1_F, 0_N\rangle + \sqrt{1/2}|0_F, 0_N\rangle$  with the storage time 10 ms.

Initial state	$g_{F-N}^{(eff)}$	$T_2^*$	$F(\text{FQ} \rightarrow \text{NV})$	$F(\text{Storage})$	$F(\text{NV} \rightarrow \text{FQ})$
$ \Phi_{1/2}\rangle$	700 kHz	90 $\mu\text{s}$	0.9689	0.9598	0.9318
		20 $\mu\text{s}$	0.9627	0.9548	0.9218
	350 kHz	90 $\mu\text{s}$	0.9421	0.9363	0.8880
		20 $\mu\text{s}$	0.9307	0.9270	0.8709
$ \Phi_1\rangle$	700 kHz	90 $\mu\text{s}$	0.9317	0.9284	0.8653
		20 $\mu\text{s}$	0.9268	0.9239	0.8562
	350 kHz	90 $\mu\text{s}$	0.8695	0.8668	0.7537
		20 $\mu\text{s}$	0.8608	0.8581	0.7386

Table II. Fidelity  $F = \sqrt{\langle \psi_t | \rho | \psi_t \rangle}$  after the transfer process with different lengths and types of the rise times for the initial states of  $|\Phi_1\rangle = |1_F, 0_N\rangle$  and  $|\Phi_{1/2}\rangle = \sqrt{1/2}|1_F, 0_N\rangle + \sqrt{1/2}|0_F, 0_N\rangle$ .

State	$g_{F-N}^{(eff)}$	$T_2^*$	rise-time func.	$F(4 \text{ ns})$	$F(10 \text{ ns})$
$ \Phi_{1/2}\rangle$	700 kHz	90 $\mu\text{s}$	exponential	0.9677	0.9647
			linear	0.9672	0.9639
		20 $\mu\text{s}$	exponential	0.9613	0.9581
			linear	0.9608	0.9573
	350 kHz	90 $\mu\text{s}$	exponential	0.9412	0.9395
			linear	0.9410	0.9392
		20 $\mu\text{s}$	exponential	0.9296	0.9278
			linear	0.9295	0.9275
$ \Phi_1\rangle$	700 kHz	90 $\mu\text{s}$	exponential	0.9294	0.9241
			linear	0.9288	0.9228
		20 $\mu\text{s}$	exponential	0.9246	0.9193
			linear	0.9240	0.9180
	350 kHz	90 $\mu\text{s}$	exponential	0.8678	0.8648
			linear	0.8677	0.8646
		20 $\mu\text{s}$	exponential	0.8591	0.8561
			linear	0.8590	0.8559

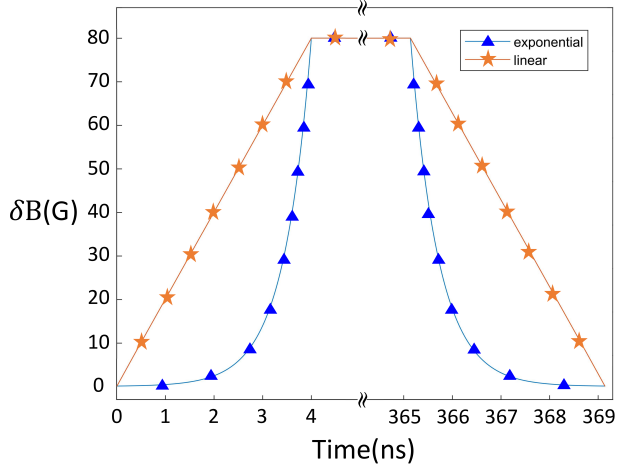


Figure 4. Temporal variation of the magnetic field with linear or exponential ramping from off-resonance (0 G) to resonance (80 G) in 4 ns at the beginning, and using an inverse ramping at the end of the state transfer stage. Only the rise-time and fall-time regimes are shown and the storage stage, during which the magnetic field is fixed, is not shown.

## V. CONCLUSION

We have demonstrated how to couple a superconducting FQ with a single electron spin of a NV-center spin via a collective KM in a ferromagnetic material, YIG. This scheme enhances the effective coupling between the FQ and the NV-center spin, allowing the single-NV-center spin to interact with the FQ at a longer spatial distance. This provides greater flexibility for the design of hybrid quantum systems. We have proposed a protocol for quantum state memory and presented a quantitative analysis of the state transfer, taking into consideration the possible decay channels and imperfect technical issues. This YIG architecture can be used not only as a quantum memory but also as a quantum transducer that couples a single-NV-center spin with other kinds of qubits or with a magnetic field.

## ACKNOWLEDGMENTS

G.D.L. and H.S.G. acknowledge support from the the Ministry of Science and Technology of Taiwan un-

der Grants No. MOST 105-2112-M-002-015-MY3 and No. MOST 106-2112-M-002-013-MY3, from the National Taiwan University under Grant No. NTU-CCP-106R891703, and from the thematic group program of the National Center for Theoretical Sciences, Taiwan. J.T. acknowledges support from the Center of Excellence in Engineered Quantum Systems.

### Appendix A: Coupling with magnons

Here we describe how the magnons in YIG couple to the FQ or the single-NV spin, and give a detailed derivation of their coupling strengths. The Hamiltonian of a FQ can be written as  $H_F = \frac{1}{2}\omega_F\sigma_F^{(z)} + \frac{1}{2}\epsilon\sigma_F^{(x)}$ , where  $\omega_F$  is the energy of the tunnel splitting,  $\epsilon = 2I_p(\Phi - \Phi_0/2)$  is the energy bias,  $I_p$  is the persistent current of the FQ,  $\Phi_0$  is the fluxon, and  $\Phi$  is the external flux. If  $\Phi$  is tuned to the optimal point with  $\Phi = \Phi_0/2$  so that  $\epsilon = 0$ , then one has  $H_F = \frac{1}{2}\omega_F\sigma_F^{(z)}$ . As discussed in the main text, the FQ-YIG coupling comes from the Zeeman-like interaction of the spins in the YIG experienced in the magnetic field  $\mathbf{B}_F(r)$  produced by the persistent current of the FQ (see Fig. 1). Since the persistent current carried by the side wire of the FQ loop near the YIG is along the  $z$  axis, the magnetic field  $\mathbf{B}_F(r) = (\frac{\mu_0}{2\pi r})I_p\sigma_F^{(x)}$  generated by this persistent current is in the  $x$  axis of the YIG [18]. Then the coupling Hamiltonian reads

$$\begin{aligned} H_{FY} &= - \sum_r \gamma_e \mathbf{B}_F(r_F) \cdot \mathbf{S}_r \\ &= - \sum_r \left( \frac{\mu_0 \gamma_e I_p}{2\pi r_F} \right) \sigma_F^{(x)} S_r^{(x)}, \end{aligned} \quad (\text{A1})$$

where  $r_F$  is the distance between a spin in the YIG and the FQ. The YIG-NV coupling Hamiltonian through the dipole-dipole interaction is written as

$$H_{YN} = - \frac{\mu_0 \gamma_e^2}{4\pi} \sum_{r_N} \frac{3(\mathbf{S}_r \cdot \hat{\mathbf{r}}_N)(\sigma_N \cdot \hat{\mathbf{r}}_N) - (\mathbf{S}_r \cdot \sigma_N)}{2r_N^3}. \quad (\text{A2})$$

Due to the external magnetic field  $B$  applied in the  $z$  direction, which makes the frequencies  $\omega_N$  and  $\gamma_e B$  much larger than the dipole-dipole coupling strength, we can apply the secular approximation to rewrite Eqs. (A2) as

$$H_{YN} = - \frac{\mu_0 \gamma_e^2 \hbar}{8\pi} \sum_r \left( \frac{3\cos^2\theta_{r_N} - 1}{r_N^3} \right) \left[ 3S_r^{(z)}\sigma_N^{(z)} - \mathbf{S}_r \cdot \sigma_N \right], \quad (\text{A3})$$

where  $r_N$  is the distance between a spin in the YIG and the NV spin, and  $\theta_{r_N}$  is the angle between the vector, which connects the NV and the spin in YIG, and the direction of the external magnetic field. We can rewrite

this Hamiltonian as  $H_{YN} \simeq H'_{YN} + H_{YN}^{(z)}$ , where

$$H'_{YN} = \sum_{r_N} \left( \frac{\mu_0 \gamma_e^2 \hbar}{4\pi} \right) \left( \frac{3\cos^2\theta_{r_N} - 1}{r_N^3} \right) \left( S_r^{(+)}\sigma_N^{(-)} + S_r^{(-)}\sigma_N^{(+)} \right), \quad (\text{A4})$$

$$H_{YN}^{(z)} = - \sum_{r_N} \left( \frac{\mu_0 \gamma_e^2 \hbar}{4\pi} \right) \left( \frac{3\cos^2\theta_{r_N} - 1}{r_N^3} \right) S_r^{(z)}\sigma_N^{(z)}. \quad (\text{A5})$$

Magnons are low-energy spin-wave excitations, which are used to describe the collective behavior of the spins in YIG. Since the system of the quantum memory is at a temperature much lower than the Curie temperature of YIG,  $T_c=559$  K, and the YIG is in an off-resonant coupling regime to the FQ and NV-center spin, one expects the excitation number to be very small. In this low-temperature and low-excitation regime, it is convenient to use the Holstein-Primakoff transformation [17, 20],

$$S_r^{(z)} = -s + a_r^\dagger a_r \approx -s, \quad (\text{A6})$$

$$S_r^{(-)} = \sqrt{2s} \sqrt{1 - \frac{n_r}{2s}} a_r \approx \sqrt{2s} a_r, \quad (\text{A7})$$

$$S_r^{(+)} = \left( S_r^{(-)} \right)^\dagger, \quad (\text{A8})$$

to transform the spin operators in the YIG into bosonic operators, where each operator is associated with a particle coordinate. Using the creation and annihilation operators of the magnon modes in the wave-vector representation,

$$a_k^\dagger = \frac{1}{\sqrt{N}} \sum_r e^{-ik \cdot r} a_r^\dagger, \quad (\text{A9})$$

$$a_k = \frac{1}{\sqrt{N}} \sum_r e^{ik \cdot r} a_r, \quad (\text{A10})$$

one can then rewrite the Hamiltonian of YIG as Eq. (6).

Since the coupling strength in  $H_{FY}$  is far smaller than  $\omega_F$  and  $\omega_Y$ , it is valid to use the RWA and Eqs. (A6)–(A10) to rewrite the FQ-YIG coupling Hamiltonian, given by Eq. (A1), as

$$\begin{aligned} H'_{FY} &= - \sum_r \left( \frac{\mu_0 \gamma_e I_p}{2\pi r_F} \right) \left( \sigma_F^{(+)} S_r^{(-)} + H.C. \right) \\ &\approx - \sum_k \left[ g_{FY}(k) \sigma_F^{(+)} a_k + H.C. \right], \end{aligned} \quad (\text{A11})$$

with the coupling strength

$$g_{FY}(k) = \frac{\mu_0 \gamma_e I_p}{2\pi} \sqrt{\frac{2s}{N}} \sum_{r_F} \frac{e^{-ik \cdot a}}{r_F}. \quad (\text{A12})$$

Similarly, the YIG-NV coupling reads

$$H'_{YN} \simeq - \sum_k \left[ g_{YN}(k) a_k^\dagger \sigma_N^{(-)} + H.C. \right] \quad (\text{A13})$$

where

$$g_{YN}(k) = -\frac{\mu_0}{4\pi}\gamma_e^2\hbar\sqrt{\frac{2s}{N}}\sum_{r_N}^N\left(\frac{3\cos^2\theta_{r_N}-1}{r_N^3}\right)e^{ik\cdot a}, \quad (\text{A14})$$

is the coupling strength between the YIG and NV-center spin. Using Eq. (A6), one can also rewrite Eq. (A5) as

$$H_{YN}^{(z)} \simeq \delta_{YN}\sigma_N^{(z)}, \quad (\text{A15})$$

where  $\delta_{YN} = \sum_{r_N} \frac{\mu_0}{4\pi}\gamma_e^2\hbar\left(\frac{3\cos^2\theta_{r_N}-1}{r_N^3}\right)s$  is the induced energy shift to the NV-center storage qubit due to the coupling with the YIG.

### Appendix B: Derivation of the effective Hamiltonian by the Schriffier-Wolff transformation

Here we describe here the procedure to derive the effective Hamiltonian between the the FQ and the NV-center spin. Following Schriffier and Wolff's approach [31–33], we can make a canonical transformation  $e^{-\eta}$  on our original Hamiltonian  $H = H_0 + H_c$ , where  $H_0 = H_s + H_{YN}^{(z)}$  with  $H_s$  defined in Eq. (1),  $H_{YN}^{(z)}$  defined in Eq. (A15), and  $H_c$  defined in Eq. (7). The Hamiltonian after the transformation reads

$$\begin{aligned} \tilde{H} &= e^\eta H e^{-\eta} \\ &= H + [\eta, H] + \frac{1}{2!}[\eta, [\eta, H]] + \dots \end{aligned} \quad (\text{B1})$$

By choosing proper operator  $\eta$  satisfying  $[H_0, \eta] = H_c$ , one has

$$\tilde{H} \simeq H_0 + \frac{1}{2}[\eta, H_c]. \quad (\text{B2})$$

In our case,

$$\eta = \lim_{\lambda \rightarrow 0} \left[ -i \int_0^\infty H_c(t) e^{-\lambda t} dt \right], \quad (\text{B3})$$

and

$$\tilde{H} \simeq H_0 - \lim_{\lambda \rightarrow 0} \frac{i}{2} \int_0^\infty [H_c(t), H_c] e^{-\lambda t} dt, \quad (\text{B4})$$

where  $H_c(t) = e^{iH_0 t} H_c e^{-iH_0 t}$ . Since the size of the YIG is small, the KM of YIG [13, 15] is gapped from the higher-energy modes. Thus, in a low-temperature and virtual-excitation regime of our scheme, we consider only the KM of the YIG to mediate the effective coupling strength between the FQ and the NV-center spin. To obtain the effective Hamiltonian between the FQ and the NV-center spin without considering the detailed dynamics of the YIG, we trace out the degrees of freedoms of the YIG, i.e.,  $H_{\text{eff}} = \langle \tilde{H} \rangle_Y$ , with  $\langle a_K^\dagger a_K \rangle_Y = n_K$  being the mean occupation number of the KM (similar to a mean-field approximation). This is a good approximation as the YIG is in a low-temperature and low-excitation regime. Since  $H_c = H'_{FY} + H'_{YN}$ , we can rewrite Eq. (B4) by categorizing the terms of the commutators after a trace over the YIG degrees of freedom into two types,

$$H_{\text{eff}} \equiv H_0 - (\delta H_s + \delta H_c) \quad (\text{B5})$$

The first type in Eq. (B5) reads

$$\delta H_s = \lim_{\lambda \rightarrow 0} \frac{i}{2} \int_0^\infty \langle [H'_{FY}(t), H'_{FY}] + [H'_{YN}(t), H'_{YN}] \rangle_Y e^{-\lambda t} dt \quad (\text{B6})$$

$$= \frac{1}{2} \delta_F \sigma_F^{(z)} + \frac{1}{2} \delta_N \sigma_N^{(z)}, \quad (\text{B7})$$

where

$$\delta_F = g_{FY}^2(\omega_K) \left( \frac{1}{\omega_F - \omega_K} \right), \quad (\text{B8})$$

$$\delta_N = g_{YN}^2(\omega_K) \left[ \frac{1}{(\omega_F + \delta_{YN}) - \omega_K} \right], \quad (\text{B9})$$

with  $\omega_K$  denoting the frequency of the KM, are the energy shifts of the qubits of the FQ and NV systems, respectively. We demonstrate how to derive Eq. (B7) from Eq. (B6) by calculating the term containing  $\delta_F$  explicitly, and then the other term containing  $\delta_N$  can be obtained in a similar way. The commutator in the first term of Eq. (B6) considering only the KM is

$$\begin{aligned}
\langle [H'_{FY}(t), H'_{FY}] \rangle_Y &= g_{FY}^2 \left\langle [\sigma_F^{(+)}(t) a_K(t), \sigma_F^{(-)} a_K^\dagger] + [\sigma_F^{(-)}(t) a_K^\dagger(t), \sigma_F^{(+)} a_K] \right\rangle_Y \\
&= g_{FY}^2 \left\langle e^{i(\omega_F - \omega_K)t} \left[ \sigma_F^{(-)} \sigma_F^{(+)} + \sigma_F^{(z)} (a_K^\dagger a_K + 1) \right] \right. \\
&\quad \left. + e^{-i(\omega_F - \omega_K)t} \left[ -\sigma_F^{(-)} \sigma_F^{(+)} - \sigma_F^{(z)} (a_K^\dagger a_K + 1) \right] \right\rangle_Y \\
&= g_{FY}^2 \left\{ e^{i(\omega_F - \omega_K)t} \left[ \sigma_F^{(-)} \sigma_F^{(+)} + \sigma_F^{(z)} (n_K + 1) \right] \right. \\
&\quad \left. + e^{-i(\omega_F - \omega_K)t} \left[ -\sigma_F^{(-)} \sigma_F^{(+)} - \sigma_F^{(z)} (n_K + 1) \right] \right\}. \tag{B10}
\end{aligned}$$

Then, integrating it over time as in Eq. (B6), one obtains

$$\begin{aligned}
\lim_{\lambda \rightarrow 0} \frac{i}{2} \int_0^\infty \langle [H'_{FY}(t), H'_{FY}] \rangle_Y e^{-\lambda t} dt &= \frac{i}{2} g_{FY}^2 \lim_{\lambda \rightarrow 0} \int_0^\infty \left\{ e^{i(\omega_F - \omega_K)t} \left[ \sigma_F^{(-)} \sigma_F^{(+)} + \sigma_F^{(z)} (n_K + 1) \right] \right. \\
&\quad \left. + e^{-i(\omega_F - \omega_K)t} \left[ -\sigma_F^{(-)} \sigma_F^{(+)} - \sigma_F^{(z)} (n_K + 1) \right] \right\} e^{-\lambda t} dt \\
&= g_{FY}^2 \lim_{\lambda \rightarrow 0} \left( \frac{1}{\omega_F - \omega_K + i\lambda} \right) \left[ \frac{1}{2} (2n_K + 1) \sigma_F^{(z)} + \frac{1}{2} I_F \right] \\
&= g_{FY}^2 \left( \frac{1}{\omega_F - \omega_K} \right) \left[ \frac{1}{2} (2n_K + 1) \sigma_F^{(z)} + \frac{1}{2} I_F \right] \\
&\simeq \frac{1}{2} g_{FY}^2 \left( \frac{1}{\omega_F - \omega_K} \right) \sigma_F^{(z)}, \tag{B11}
\end{aligned}$$

where the constant energy term containing the identity operator  $I_F$  can be ignored, and  $n_K \rightarrow 0$  since the system is operated in a virtual-excitation regime. Equation (B11) is the first term of Eq. (B7). Similarly, the second term of Eq. (B6) can be calculated and yields the term containing  $\delta_N$  in Eq. (B7).

The other type  $\delta H_c$  in Eq. (B5) represents the effective coupling between the FQ and NV-center spin:

$$\delta H_c = \lim_{\lambda \rightarrow 0} \frac{i}{2} \int_0^\infty \langle [H'_{FY}(t), H'_{YN}] + [H'_{YN}(t), H'_{FY}] \rangle_Y e^{-\lambda t} dt \tag{B12}$$

$$= g_{FN, \text{eff}} \left( \sigma_F^{(+)} \sigma_N^{(-)} + H.C. \right), \tag{B13}$$

with

$$g_{FN, \text{eff}} = \frac{1}{2} g_{FY}(K) g_{YN}(K) \left[ \frac{1}{\omega_F - \omega_K} + \frac{1}{(\omega_N + \delta_{YN}) - \omega_K} \right]. \tag{B14}$$

We now show how to obtain Eq. (B13) from Eq. (B12). Following the same approach as in Eqs. (B10) and (B11), the first term of the commutator in Eq. (B12) reads

$$\begin{aligned}
\lim_{\lambda \rightarrow 0} \frac{i}{2} \int_0^\infty \langle [H'_{FY}(t), H'_{YN}] \rangle_Y e^{-\lambda t} dt &= \lim_{\lambda \rightarrow 0} \frac{i}{2} \int_0^\infty g_{FY} g_{YN} \left\langle [\sigma_F^{(+)}(t) a_K(t), a_K^\dagger \sigma_N^{(-)}] + [\sigma_F^{(-)}(t) a_K^\dagger(t), a_K \sigma_N^{(+)}] \right\rangle_Y e^{-\lambda t} dt \\
&= \frac{i}{2} g_{FY} g_{YN} \lim_{\lambda \rightarrow 0} \int_0^\infty \left[ e^{i(\omega_F - \omega_K)t} \left( \sigma_F^{(+)} \sigma_N^{(-)} \right) + e^{-i(\omega_F - \omega_K)t} \left( -\sigma_F^{(-)} \sigma_N^{(+)} \right) \right] e^{-\lambda t} dt \\
&= g_{FY} g_{YN} \lim_{\lambda \rightarrow 0} \left[ \frac{1}{2} \left( \frac{1}{\omega_F - \omega_K + i\lambda} \right) \sigma_F^{(+)} \sigma_N^{(-)} + \frac{1}{2} \left( \frac{1}{\omega_F - \omega_K - i\lambda} \right) \sigma_F^{(-)} \sigma_N^{(+)} \right] \\
&= \frac{1}{2} g_{FY} g_{YN} \left( \frac{1}{\omega_F - \omega_K} \right) \left( \sigma_F^{(+)} \sigma_N^{(-)} + \sigma_F^{(-)} \sigma_N^{(+)} \right). \tag{B15}
\end{aligned}$$

The second term of the commutator in Eq. (B12) can be evaluated in a similar way and combining with Eq. (B15) give the results of Eqs. (B13) and (B14). Combining all these results, one arrives at the effective Hamiltonian of Eq. (12).

[1] J. Clarke and F. K. Wilhelm, Nature (London) **453**, 1031 (2008).

[2] Z.-L. Xiang, S. Ashhab, J. Q. You, and F. Nori, Rev.

- Mod. Phys. **85**, 623 (2013).
- [3] M. W. Doherty, N. B. Manson, P. Delaney, F. Jelezko, J. Wrachtrup, and L. C. Hollenberg, *Physics Reports* **528**, 1 (2013).
- [4] J. Twamley and S. D. Barrett, *Phys. Rev. B* **81**, 241202 (2010).
- [5] Y. Kubo, F. R. Ong, P. Bertet, D. Vion, V. Jacques, D. Zheng, A. Dréau, J.-F. Roch, A. Auffeves, F. Jelezko, J. Wrachtrup, M. F. Barthe, P. Bergonzo, and D. Esteve, *Phys. Rev. Lett.* **105**, 140502 (2010).
- [6] Y. Kubo, C. Grezes, A. Dewes, T. Umeda, J. Isoya, H. Sumiya, N. Morishita, H. Abe, S. Onoda, T. Ohshima, V. Jacques, A. Dréau, J.-F. Roch, I. Diniz, A. Auffeves, D. Vion, D. Esteve, and P. Bertet, *Phys. Rev. Lett.* **107**, 220501 (2011).
- [7] X.-Y. Lü, Z.-L. Xiang, W. Cui, J. Q. You, and F. Nori, *Phys. Rev. A* **88**, 012329 (2013).
- [8] X. Zhu, S. Saito, A. Kemp, K. Kakuyanagi, S.-i. Karimoto, H. Nakano, W. J. Munro, Y. Tokura, M. S. Everitt, K. Nemoto, M. Kasu, N. Mizuochi, and K. Semba, *Nature (London)* **478**, 221 (2011).
- [9] V. Cherepanov, I. Kolokolov, and V. L'vov, *Physics Reports* **229**, 81 (1993).
- [10] A. A. Serga, A. V. Chumak, and B. Hillebrands, *Journal of Physics D: Applied Physics* **43**, 264002 (2010).
- [11] L. Trifunovic, F. L. Pedrocchi, S. Hoffman, P. Maletinsky, A. Yacoby, and D. Loss, *Nat. Nanotechnol.* **10**, 541 (2015).
- [12] Y. Tabuchi, S. Ishino, T. Ishikawa, R. Yamazaki, K. Usami, and Y. Nakamura, *Phys. Rev. Lett.* **113**, 083603 (2014).
- [13] D. Zhang, X.-M. Wang, T.-F. Li, X.-Q. Luo, W. Wu, F. Nori, and J. Q. You, *Npj Quantum Inf.* **1**, 15014 (2015).
- [14] V. V. Kruglyak, S. O. Demokritov, and D. Grundler, *Journal of Physics D: Applied Physics* **43**, 264001 (2010).
- [15] Y. Tabuchi, S. Ishino, A. Noguchi, T. Ishikawa, R. Yamazaki, K. Usami, and Y. Nakamura, *Science* **349**, 405 (2015).
- [16] R. Hisatomi, A. Osada, Y. Tabuchi, T. Ishikawa, A. Noguchi, R. Yamazaki, K. Usami, and Y. Nakamura, *Phys. Rev. B* **93**, 174427 (2016).
- [17] L. Trifunovic, F. L. Pedrocchi, and D. Loss, *Phys. Rev. X* **3**, 041023 (2013).
- [18] T. Douce, M. Stern, N. Zagury, P. Bertet, and P. Milman, *Phys. Rev. A* **92**, 052335 (2015).
- [19] J. Norpoth, S. Dreyer, and C. Jooss, *Journal of Physics D: Applied Physics* **41**, 025001 (2008).
- [20] T. Holstein and H. Primakoff, *Phys. Rev.* **58**, 1098 (1940).
- [21] Y. Tabuchi, S. Ishino, A. Noguchi, T. Ishikawa, R. Yamazaki, K. Usami, and Y. Nakamura, *Comptes Rendus Physique* **17**, 729 (2016).
- [22] H. Carmichael, *Statistical Methods in Quantum Optics 1: Master Equations and Fokker-Planck Equations*, *Physics and Astronomy Online Library* (Springer-Verlag, Berlin-Heidelberg, 1999).
- [23] M. Stern, G. Catelani, Y. Kubo, C. Grezes, A. Bienfait, D. Vion, D. Esteve, and P. Bertet, *Phys. Rev. Lett.* **113**, 123601 (2014).
- [24] T. Ishikawa, K.-M. C. Fu, C. Santori, V. M. Acosta, R. G. Beausoleil, H. Watanabe, S. Shikata, and K. M. Itoh, *Nano Lett.* **12**, 2083 (2012).
- [25] N. Bar-Gill, L. M. Pham, A. Jarmola, D. Budker, and R. L. Walsworth, *Nature Communications* **4**, 1743 (2013).
- [26] C. Hahn, V. V. Naletov, G. de Loubens, O. Klein, O. d'Allivy Kelly, A. Anane, R. Bernard, E. Jacquet, P. Bortolotti, V. Cros, J. L. Prieto, and M. Muñoz, *Appl. Phys. Lett.* **104**, 152410 (2014).
- [27] O. Klein, (private communication) (2018).
- [28] F. Yan, S. Gustavsson, A. Kamal, J. Birenbaum, A. P. Sears, D. Hover, T. J. Gudmundsen, D. Rosenberg, G. Samach, S. Weber, J. L. Yoder, T. P. Orlando, J. Clarke, A. J. Kerman, and W. D. Oliver, *Nature Communications* **7**, 12964 (2016).
- [29] C. Kittel, *Introduction to Solid State Physics, 8th ed.* (Wiley, New York, 2004).
- [30] T. A. Salaoru and J. R. Woodward, *Review of Scientific Instruments* **78**, 036104 (2007).
- [31] J. R. Schrieffer and P. A. Wolff, *Phys. Rev.* **149**, 491 (1966).
- [32] M. M. Salomaa, *Phys. Rev. B* **37**, 9312 (1988).
- [33] S. Bravyi, D. P. DiVincenzo, and D. Loss, *Annals of Physics* **326**, 2793 (2011).